Propulsion and Power Research 2013;2(3):177–187

http://ppr.buaa.edu.cn/

Propulsion and Power Research

www.sciencedirect.com

ORIGINAL ARTICLE

Investigation on heat transfer enhancement and pressure loss of double swirl chambers cooling

Gang Lin[a,*], Karsten Kusterer[a], Dieter Bohn[b], Takao Sugimoto[c], Ryozo Tanaka[c], Masahide Kazari[d]

[a]B&B-AGEMA GmbH, Juelicher Str.338, Aachen 52070, Germany
[b]RWTH Aachen University, Templergraben 55, Aachen 52056, Germany
[c]Kawasaki Heavy Industries, LTD., Gas Turbine & Machinery Company, Akashi 673-8666, Japan
[d]Kawasaki Heavy Industries, LTD., Technical Institute, Akashi 673-8666, Japan

Received 22 April 2013; accepted 17 June 2013
Available online 27 August 2013

KEYWORDS

Gas turbine;
Internal cooling;
Double swirl chambers;
Thermal performance;
Heat transfer enhancement

Abstract By merging two standard swirl chambers, an alternative cooling configuration named double swirl chambers (DSC) has been developed. In the DSC cooling configuration, the main physical phenomena of the swirl flow in swirl chamber and the advantages of swirl flow in heat transfer augmentation are maintained. Additionally, three new physical phenomena can be found in DSC cooling configuration, which result in a further improvement of the heat transfer: (1) impingement effect has been observed, (2) internal heat exchange has been enhanced between fluids in two swirls, and (3) "∞" shape swirl has been generated because of cross effect between two chambers, which improves the mixing of the fluids. Because of all these improvements, the DSC cooling configuration leads to a higher globally-averaged thermal performance parameter ($\overline{\overline{Nu}}/Nu_\infty/(f/f_0)^{1/3}$) than standard swirl chamber. In particular, at the inlet region, the augmentation of the heat transfer is nearly 7.5 times larger than the fully developed non-swirl turbulent flow and the circumferentially averaged Nusselt number coefficient is 41% larger than the standard swirl chamber. Within the present work, a further investigation on the DSC cooling configuration has been focused on the influence of geometry parameters e.g. merging ratio of chambers and aspect ratio of inlet duct on the cooling performance. The results show a very large influence of these geometry parameters in

*Corresponding author: Tel.: +49 241 5687840.
E-mail address: lin@bub-agema.de (Gang Lin).

Peer review under responsibility of National Laboratory for Aeronautics and Astronautics, China.

Production and hosting by Elsevier

http://dx.doi.org/10.1016/j.jppr.2013.07.003

heat transfer enhancement and pressure drop ratio. Compared with the basic configuration of DSC cooling, the improved configuration with 20% to 23% merging ratio shows the highest globally-averaged thermal performance parameter. With the same cross section area in tangential inlet ducts, the DSC cooling channel with larger aspect ratio shows larger heat transfer enhancement and at the same time reduced pressure drop ratio, which results in a better globally-averaged thermal performance parameter.

1. Introduction

In order to achieve high process efficiency for economic operation of stationary gas turbines and aero engines, extremely high turbine inlet temperatures at adjusted pressure ratios are applied. The allowable hot gas temperature is limited by the material temperature of the hot gas path components, in particular the vanes and blades of the turbine. Thus, intensive cooling is required to guarantee an acceptable life span of these components.

Huge number of techniques to enhance the convective heat transfer rates for internal cooling of turbine airfoils have been developed in recent years, e.g. rib turbulators, pin fins, dimpled surfaces, impingement cooling and swirl chambers. According to Ligrani et al. [1] and Ligrani [2], the common points of all these techniques are that they all can increase secondary flows and turbulence levels to enhance the mixing of the flows. The state of the art internal cooling technique is a combination of rib turbulators, pin fins and impingement cooling. The room for improvement, however, continues to shrink after decades of development. Facing the challenge of continuously growing temperature at turbine inlet, the development of some new cooling configurations that can provide much higher heat transfer rates has become necessary, and swirl chamber belong to one of the most recent and attractive cooling concepts.

Swirl chambers is a kind of internal flow passage, in which large-scale swirling of the flow, which circles under most circumstances around the main axis, is generated by internal inserts or outlets configurations [3]. Swirl introduced in tube flow that can enhance the surface heat transfer rates was first put forward by Kreith and Margolis [4]. In this concept, the swirl is generated during many tangential injection of the fluid at various locations along the tube axis. Hay and West [5] first proposed that the swirl chambers can be introduced in turbine blade internal cooling. In their experimental study, the swirl was produced by a single tangential slot, which was 90 degrees to the pipe axis. The results showed the heat transfer augmentation factor about eight times of the value for fully developed axial turbulent flow near the inlet region. More recently, Chang and Dhir [6,7] experimentally studied the heat transfer augmentation of swirl flows generated by six symmetrical tangential injectors at inlet. Their obtained data showed a very large anisotropy in eddy viscosity and two major mechanisms for enhancement of heat transfer: (1) high axial velocity near the wall increases the wall heat flux; (2) high turbulence level promotes the mixing. In the experiment studied by Khalatov et al. [8,9] the swirl chambers were used to cool a blade leading edge. Khalatov et al. [10] used swirl chambers in three passages cooling channel, where only passages No. 2 and No. 3 contain swirl flows. Ligrani et al. [11], Thambu et al. [12], Hedlund et al. [13] and Hedlund and Ligrani [14] studied the swirl chambers with the same configuration, which had two tangential inlet slots at different locations along the tube axis. They used smoke injection to visualize flow and vortex structures. The results showed a relation between Görtler vortex pairs near the concave surface of chamber and the heat transfer augmentation. Ling et al. [15] used similar geometry of test facility as the one used in Ligrani [11] to compare the heat transfer augmentation between swirl chambers and impingement cooling. At a low mass flow rate, the impingement cooling was more effective. With increased mass flow the swirl chambers showed better performance than impingement cooling. Besides, the swirl chambers had a more uniform heat transfer distribution. Liu [16] presented a numerical study on the experimental geometry investigated by Hay and West [5] and Ling et al. [15]. The results of calculation with turbulence model SST $k-\omega$ showed the best agreement compared with other turbulence models used. All the turbulence models presented significant underestimation of the Nusselt number and swirl number at the region from the second half to the outlet in the case of Hay and West [5]. Hwang and Cheng [17] investigated the swirl flow in a triangular duct to enhance the heat transfer rates at blade leading edge. The cooling concept by Segura and Acharya [18–20] presented a configuration to generate swirl flow in a channel with a 3:1 aspect ratio. In this configuration, the swirl was generated by introducing tangential jets along the side walls of the main coolant passage. Lerch et al. [21] experimentally studied the impact of swirl chambers on adiabatic film cooling. This investigation indicated that the swirl chambers can obviously alter the film cooling behavior. Wassermann [22] experimentally studied the heat transfer enhancement of a two passage swirl chambers with a 180° bend. Kusterer et al. [23] numerically investigated the heat transfer enhancement of swirl flows in double swirl chambers, which were generated by merging of two swirl chambers.

Nomenclature

A_r	aspect ratio of inlet slot
b	width of inlet slot (unit: m)
d	height of inlet slot (unit: m)
D	swirl chamber diameter (unit: m)
D_h	hydraulic diameter (unit: m)
f	friction factor
f_0	friction factor for fully developed non-swirling flow in chamber
G_θ	local axial flux of angular momentum (unit: $kg \cdot m/s^2$)
G_x	local axial flux of linear momentum (unit: $kg \cdot m/s^2$)
h	heat transfer coefficient (unit: $W/(m^2 \cdot K)$)
L	length of swirl chamber (unit: m)
L_1	length of inlet duct (unit: m)
L_2	distance between two centres in DSC (unit: m)
M_r	merging ratio of two chambers
Nu	Nusselt number based on hydraulic diameter
Nu_∞	Nusselt number for fully developed non-swirling flow in chamber
P_s	static pressure (unit: Pa)
P_t	total pressure (unit: Pa)
P_w	static wall pressure (unit: Pa)
Pr	Prandtl number
q_w	wall heat flux (unit: W/m^2)
r	radius in swirl chamber (unit: m)
R	inside radius of swirl chamber (unit: m)
Re_h	Reynolds number based on hydraulic diameter
S	swirl number
T_b	mass averaged air bulk temperature (unit: K)
T_j	jet inlet air temperature (unit: K)
T_w	wall surface temperature (unit: K)
u	axial velocity of the stream in swirl flow (unit: m/s)
U	mean axial velocity (unit: m/s)
v	tangential velocity of the stream in swirl flow (unit: m/s)
X	swirl chamber axial distance (unit: m)
$y+$	non-dimensional wall distance

Greek letters

λ	thermal conductivity (unit: $W/(m \cdot K)$)
ρ	density of fluid (unit: kg/m^3)
k	turbulent kinetic energy (unit: m^2/s^2)
ω	specific turbulence dissipation rate (unit: s^{-1})

Abbreviation

CFD	computational fluid dynamics
DSC	double swirl chambers
SC	swirl chamber

This cooling concept presented even higher locally and globally-averaged heat transfer coefficient than the values in standard swirl chamber.

In the present study, the influence of geometry parameters, e.g. merging ratio of chambers and aspect ratio of inlet duct on the cooling performance have been numerically investigated for the DSC cooling configuration. At first, a systematic numerical study in swirl flow in tube is presented. The experimental geometry investigated by Hay and West [5] has been chosen as the physical models for this comparative calculation. Several different turbulence models have been used for the calculations with STAR CCM+, showing significant variations in the heat transfer prediction. After that, the DSC cooling has been studied in numerical under the same flow Reynolds number and the same boundary conditions but with different geometry parameters. Based on the numerical study, an improved configuration of the DSC cooling with higher globally-averaged thermal performance parameter has been performed.

2. Computational setup

2.1. Geometry

The experimental geometry investigated by Hay and West [5] has been chosen for the validation, which is illustrated in Figure 1. In this case, the swirl flow in the tube is generated only by the tangential single inlet slot without any inserts. A summary of the geometrical details can be found in Table 1.

Figure 2 presents a schematic description of the DSC-cooling configuration, which is generated by merging of two swirl chambers. After the merging of two chambers, the distance between two centers is smaller than one diameter. The merging ratio is defined as

$$M_r = \frac{D - L_2}{D} \tag{1}$$

to describe the overlap of two chambers. Apart from the cross section, all the other geometries e.g. inlet duct length, diameter and chamber length are the same as in the test case by Hay and West [5]. The geometry parameters in DSC cooling configuration which have been investigated are the merging ratio of two chambers and the aspect ratio of inlet

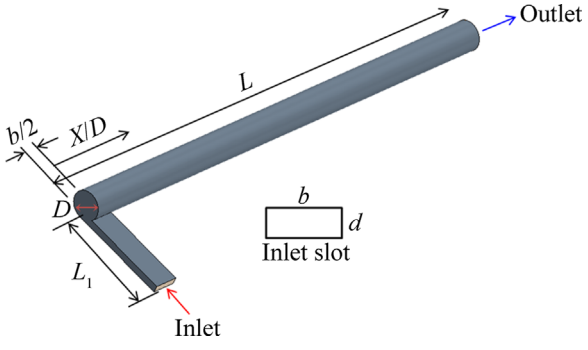

Figure 1 Geometry investigated by Hay and West [5].

duct. For the configurations with different aspect ratios, the area of the cross section for inlet duct is always the same. All the investigated cases are listed in Table 2.

Table 1 Geometry details swirl chamber investigated by Hay and West [5].

D/mm	50.8
L/mm	914
L_1/mm	175
Width *b*/mm	45.7
Height *d*/mm	12.15

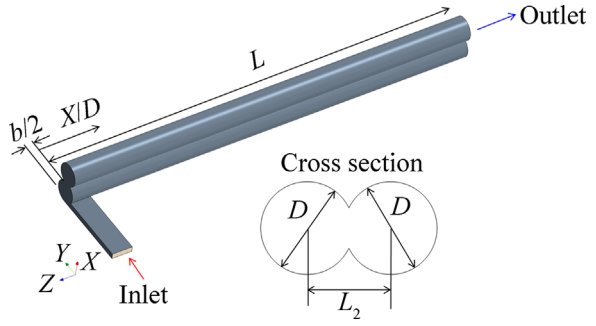

Figure 2 Schematic diagram of the double swirl chambers cooling configuration.

Table 2 Investigated cases for DSC-configurations.

Case No.	Merging ratio [-]	Aspect ratio [-]	Hydraulic diameter/mm
Case 1	5%	3.76	56.14
Case 2	10%	3.76	58.21
Case 3	15%	3.76	59.59
Case 4	20%	3.76	60.56
Case 5	23%	3.76	60.99
Case 6	25%	3.76	61.22
Case 7	27%	3.76	61.41
Case 8	30%	3.76	61.62
Case 9	35%	3.76	61.81
Case 10	25%	2	61.22
Case 11	25%	5	61.22

2.2. *Numerical method and boundary conditions*

A commercial CFD code STAR CCM+ has been applied for all the numerical investigations. Figure 3 presents the unstructured mesh in the cross sections of both cooling configurations. Unstructured polyhedral grids for calculation regions and prism layers in the near-wall region have been generated in STAR CCM+. A mesh independence study with 0.67 million, 1.45 million and 2.95 million cell numbers has been conducted for the test case by Hay and West [5]. The results showed that the suitable mesh size fell within the range of 1.45 million cells. The y^+ value of the first cell in the boundary layers is overall less than one. Stretch ratio in the development of the prism layers in normal direction of the wall surface has been controlled to be around 1.2. The same mesh setup has also been used for calculation of DSC-configuration, which results in about 2.89 million cells.

In the test by Hay and West [5], the fluid is air, which has been heated to 75 °C before entering the inlet duct. Constant temperature with $T_w = 288.15$ K is given at the chamber wall, which means the fluid has been cooled through the chamber. The end of the swirl chamber is directly open to the atmosphere. In the present study, the test condition with flow Reynolds number 10500 has been chosen for the numerical validation (Table 4). After that, for the numerical investigation of DSC-cooling, the mass flow has been adjusted in such a way that the Reynolds number Re_h is always 10500. The inlet total temperature and the outlet static pressure are both matched with those in experiment. Only the constant temperature at the chambers wall is defined with $T_j/T_w = 0.83$, which is close to engine conditions ($T_j = 348.15$ K, $T_w = 419.15$ K). Table 3 presents the boundary conditions for all the investigated cases.

3. Results and analysis

3.1. *Validation of the numerical approach*

The numerical validations have been conducted with several different turbulence models: SST *k-ω* model, realizable *k-ε* model and V2F model. The results of predictions

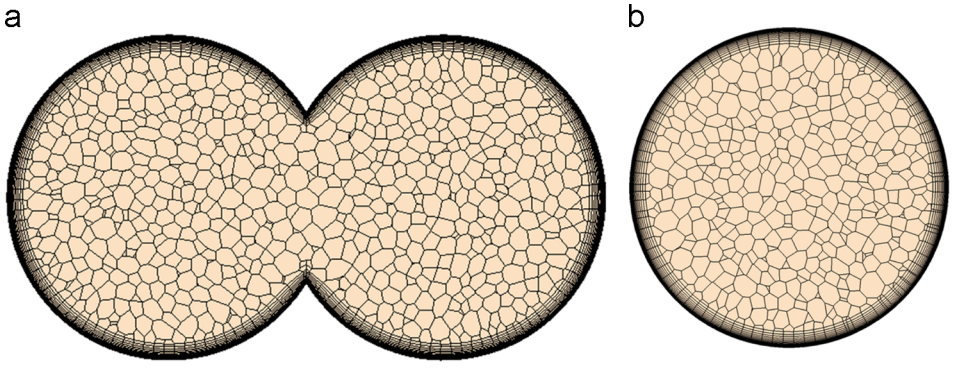

Figure 3 Mesh at the cross section *X*/*D* = 7.5 for (a) DSC-configuration and (b) SC-configuration.

Table 3 Boundary conditions for all investigated cases.

	SC (validation)	SC-cooling	DSC-cooling (all cases)
Chamber wall temperature/K	288.15	419.15	419.15
Cooling air total temperature/K	348.15	348.15	348.15
Outlet pressure/bar	1	1	1

Table 4 Flow conditions for all investigated cases.

	Air mass flow rate *m*/(g/s)	Mean axial velocity/(m/s)	Hydraulic Reynolds number [-]
SC (validation)	8.5	4.15	10500
SC-cooling	8.5	4.15	10500
DSC merging ratio 5%	15.3	3.75	10500
DSC merging ratio 10%	14.6	3.62	10500
DSC merging ratio 15%	14.0	3.54	10500
DSC merging ratio 20%	13.5	3.48	10500
DSC merging ratio 23%	13.3	3.45	10500
DSC merging ratio 25%	13.1	3.44	10500
DSC merging ratio 27%	12.9	3.43	10500
DSC merging ratio 30%	12.7	3.42	10500
DSC merging ratio 35%	12.3	3.41	10500

have been compared with the experimental data by Hay and West [5].

To characterize the intensity of swirl flow, swirl number is employed. It is defined as the ratio of the angular momentum to linear momentum flux:

$$S = \frac{G_\theta}{G_x R} = \frac{2\pi \int_0^R \rho r^2 u v \mathrm{d}r}{2\pi R \int_0^R \rho r u^2 \mathrm{d}r} \tag{2}$$

For this test case, Hay and West [5] had developed a correlation for the development of swirl numbers along the axial distance

$$S = 1.72\exp(-0.04X/D) \tag{3}$$

Figure 4 presents the comparison of the swirl number prediction by different turbulence models with experimental data. The results of numerical calculations present a right tendency of the swirl number along the axial direction as in experiment but with too steep gradient. As investigated by Kusterer et al. [23], the reason is that in the numerical

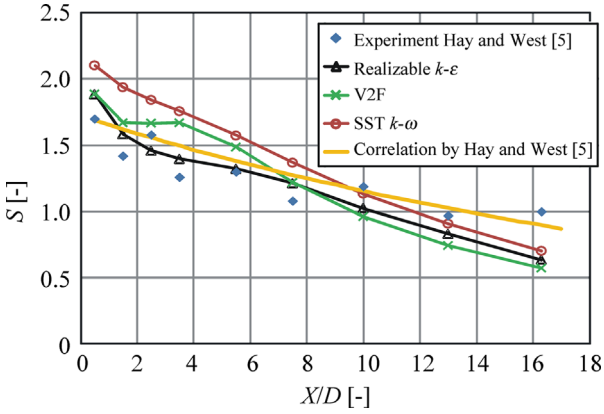

Figure 4 Comparison of the swirl number prediction by different turbulence models with experimental data by Hay and West [5].

calculations, the maximum tangential velocity decays much faster with axial distance than it does in the experiment. Due to the decay of the swirl, the core region shrinks in experiment, but this effect cannot be predicted in the numerical investigation. According to Chang and Dhir [6] and Kitoh [24], the main reason behind this difference is that the swirl flow in the annular region between the core and wall region is highly anisotropic, which is why the isotropic turbulence models cannot predict it accurately. In swirl flow there is always a very important phenomenon: the existence of reverse flow in the central region. Due to the reversal region, the cross-sectional flow area is reduced causing the axial velocity and mass flow density near the wall to increase, which in turn improves the heat transfer augmentation. In Kusterer et al. [23] the reverse flow can only be predicted from inlet to axial location $X/D=3.5$ of the chamber, after that section no reversal region can be predicted in the numerical calculations. It is the result of too fast decay of the swirl flow in the numerical calculations.

In the investigations of internal cooling, the Nusselt number ratio (Nu/Nu_∞) is always employed to characterize the heat transfer augmentation. The local Nusselt number can be calculated as

$$Nu = \frac{hD}{\lambda} = \frac{q_w D}{(T_w - T_b)\lambda} \tag{4}$$

The value Nu_∞ is defined as Nusselt number for fully developed non-swirling turbulent flow in the pipe from the Dittus-Boelter correlation

$$Nu_\infty = 0.023 Re_h^{0.8} Pr^n \tag{5}$$

where n is equal to 0.4 while heating the fluid, and 0.3 for cooling the fluid. In this test case, the swirling flow was cooled.

Figure 5 presents a comparison of the circumferentially averaged Nusselt number ratio predicted by different turbulence models with the experimental data. It can be found in the experimental data that the Nusselt number ratio decays exponentially with axial distance. At the inlet region, the heat transfer augmentation can be as high as

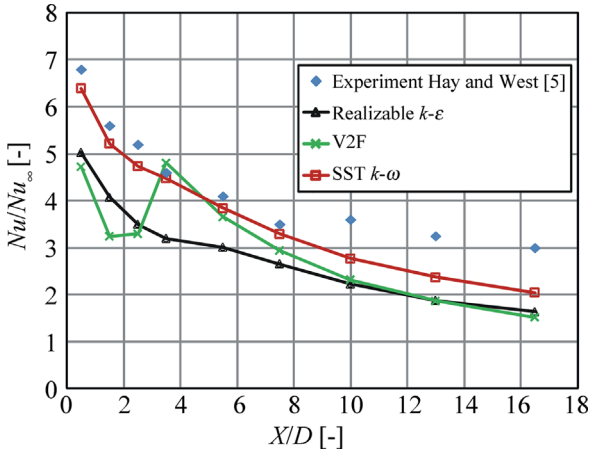

Figure 5 Comparison of circumferentially averaged Nusselt number ratio presented by different turbulence models with experimental data by Hay and West [5].

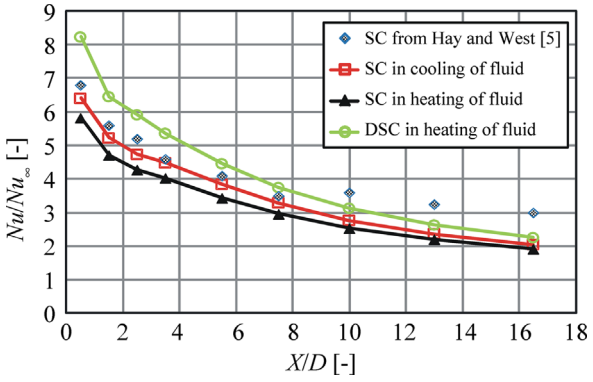

Figure 6 Comparison of circumferentially averaged Nusselt number ratio between two cooling configurations.

seven times the value for non-swirl turbulent flow. According to the numerical investigations, the results of SST k-ω model agrees the best with the experimental data in all the three turbulence models, especially at the first half chamber from inlet to the middle, but an obvious under prediction can still be found at the second half chamber, which should be the results of too fast decay of swirl in numerical calculation [23]. Thus, all the following results presented are all based on the application of SST k-ω turbulence model.

3.2. *Double swirl chambers cooling*

As mentioned before, constant temperature is given at the chambers wall in DSC-cooling with $T_w = 419.15$ K. For the comparability between two configurations the simulation of swirl chambers should be calculated again in heating of the fluid with the same T_w as in the numerical study of DSC-cooling. Figure 6 presents the comparison of circumferentially averaged Nusselt number ratio between two cooling configurations. The Nusselt number ratio with DSC-cooling is overall larger than the values with SC-cooling, especially at the inlet region the DSC-cooling configuration has a higher circumferentially averaged heat transfer coefficient in one section by approximately 41%. The major physical phenomena in the DSC-cooling and the main reasons for the improvement of heat transfer have been explained by Kusterer et al. [23]:

(1) The reattachment of the flow with the maximum velocity at the red zone in Figure 7 has an impingement effect and at downstream of reattachment a restart of the boundary layer occurs, which results in a very high local heat transfer coefficient.
(2) In the shared section A-A the heat exchange between two swirl flows has been enhanced.
(3) There is a cross effect between two swirl flows, which can lead to a very good mixing of the fluids. Because of the cross effect, a three-dimensional "∞" shape swirl flow can be generated in DSC-cooling configuration.

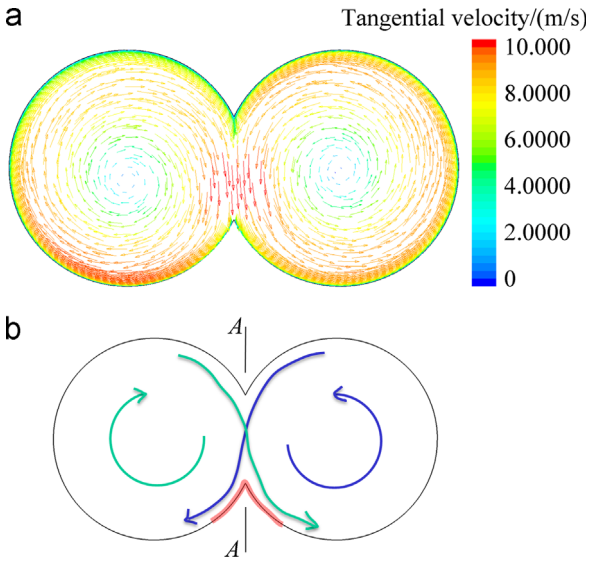

Figure 7 (a) Tangential velocity distribution in cross section at axial distance $X/D = 7.5$ and (b) schematic of the swirl flow in double swirl chambers cooling.

In the study by Kusterer et al. [23] the investigated DSC-cooling configuration has a merging ratio of 10%. In this paper, the influences of geometry parameters merging ratio and aspect ratio have been investigated and will be discussed in the following chapters.

3.2.1. *Merging ratio*

Figure 8 presents the circumferentially averaged Nusselt number ratio for the SC-cooling configuration and DSC-cooling configurations with different merging ratios. At the inlet region, all the DSC-configurations show much higher heat transfer rate than that in SC-configuration. In DSC-configurations, the Nusselt number ratio decays much faster than in SC-configuration. With a smaller merging ratio than 20%, the Nusselt number ratio in DSC-configuration is

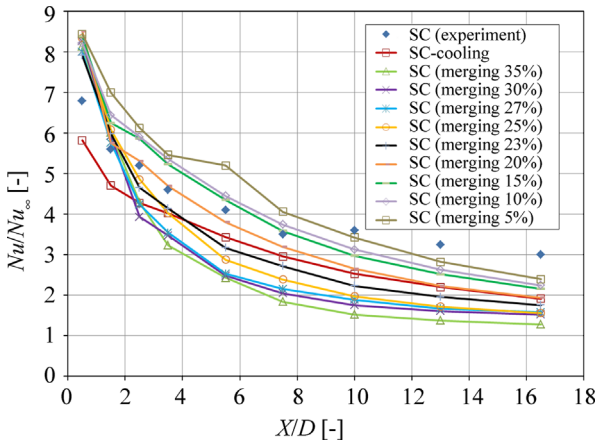

Figure 8 Comparison of circumferentially averaged Nusselt number ratio among DSC-configurations with different merging ratios.

overall larger than in SC-configuration. Lower merging ratio always leads to larger Nusselt number ratio, which also means better heat transfer rate. The reason can be found in the appendix. The appendix presents the tangential velocity distributions at the section $X/D=7.5$ from calculations with different merging ratios. A lower merging ratio means that the configuration of DSC near the shared section *A-A* is much closer to two independent swirl chambers, which also means the influence between two swirls is less and the structure of typical swirl flow can be more maintained in two chambers. The calculation result for merging ratio of 35% shows a very complex fluid structure but not two swirls. In the right chamber, a separation region can be found, and the reattachment point of the flows is not near the shared section *A-A*. With decreased merging ratio, the two swirls are more symmetry between each other. Due to the destroy of the structure of swirl in large merging ratios, the fluids decay much faster, which leads to much smaller amounts of tangential velocities at the same section along the axial direction.

Except the heat transfer rate pressure drop is another very important criterion in development of internal cooling configuration. Figure 9 shows static pressure, total pressure and wall static pressure along the axial distance from calculations with different merging ratios. Massflow averaged static pressure and total pressure are non-dimensionalized using $\rho U^2/2$ in Figures 9(a) and (b). Circumferential surface averaged wall static pressure is nondimensionalized using $\rho U^2/2$ in Figure 9(c). It can be found in these figures, the amounts of pressure drops are quite different among static, total and wall static pressure, but the influence of merging ratios is the same. Increased merging ratio always results in smaller pressure drop. Since the merging ratio is larger than 23%, the decreasing of the pressure drop is neglectful. Some deviations can still be found between $X/D=2$ and $X/D=6$, but the whole pressure drop from cross section just after inlet tube to the outlet is almost the same. The SC-configuration has a similar level of pressure drop as the DSC-configuration with merging ratio of 15%.

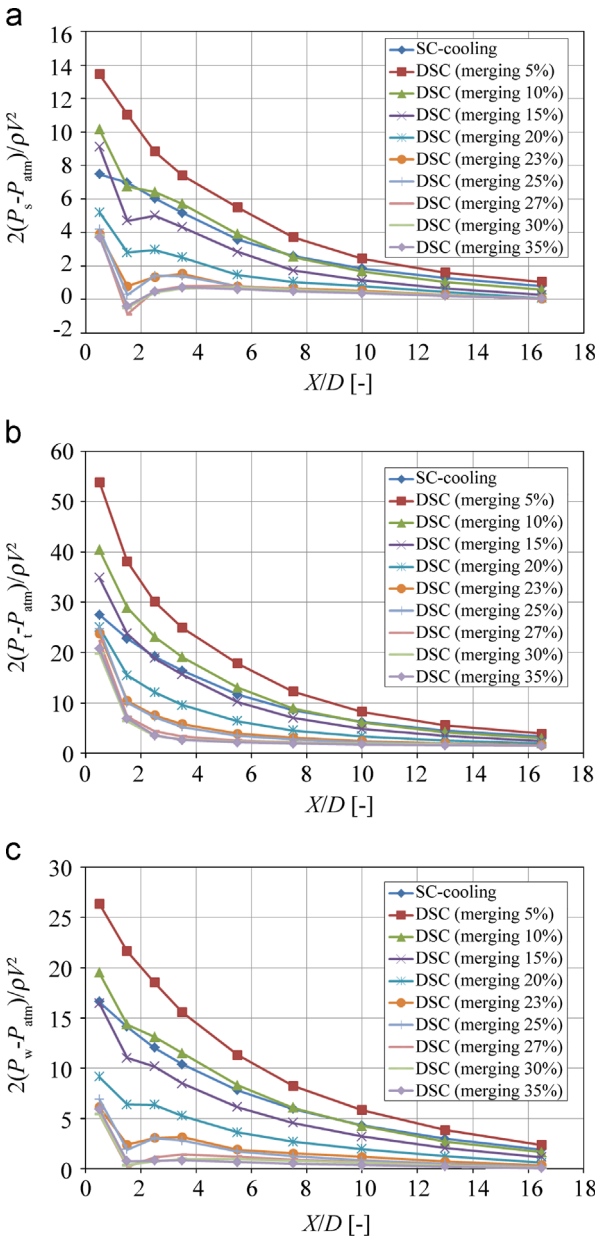

Figure 9 Pressure distributions along the axial direction. (a) Normalized static pressure, (b) normalized total pressure and (c) normalized wall static pressure for DSC-configurations with different merging ratios.

For the comparison of different internal cooling configurations, the friction factor f/f_0 is always employed to present the pressure loss. In the friction factor ratio f/f_0 the pressure drop coefficient f is defined as

$$f=\frac{\Delta P}{\frac{\frac{L}{D_h}\rho u^2}{2}} \tag{6}$$

and the baseline friction factor in a smooth channel f_0 is defined after the Blasius correlation as

$$f_0=\frac{0.3164}{Re_h^{0.25}} \tag{7}$$

which gives the best representation of friction factor data of available formulations for $Re_h < 100 \times 10^3$ [25]. According to Khalatov et al. [9], the wall static pressure drop was used to calculate the friction factor in a swirl chamber. Kunstmann et al. [26] used static pressure drop to calculate the friction factor for a rectangular internal cooing channel. By Rau et al. [27], the total pressure drop was applied to study the friction factor for cooling channel with ribs. In this paper, all these three applications have been applied to compare the pressure drops among different DSC-configurations and SC-configuration.

Globally-averaged thermal performance parameter, $\overline{\overline{Nu}}/Nu_\infty/(f/f_0)^{1/3}$, defined as the ratio of heat transfer augmentation to a smooth channel with the same pumping power, is frequently used to compare different internal cooling technology or the same technology with different geometry. Table 5 presents the calculated Nusselt number ratio, friction factor ratio and globally-averaged thermal performance of different DSC-configurations in comparison with the reference SC-configuration, in which all the values are assumed to be unities. It can be found in this table, the optimal merging ratio for DSC-configuration is always in the range of 20% to 23% for all of the three pressure drop applications.

Table 5 Comparison of Nusselt number ratio, friction factor ratio and globally-averaged thermal performance factor for DSC-configurations with different merging ratios.

Configurations	$\overline{\overline{Nu}}/Nu_\infty$	f/f_0			$\overline{\overline{Nu}}/Nu_\infty/(f/f_0)^{1/3}$		
		Static	Total	Wall	Static	Total	Wall
SC-cooling	1	1	1	1	1	1	1
DSC (5%)	1.441	2.051	2.282	1.804	1.134	1.094	1.183
DSC (10%)	1.344	1.642	1.772	1.391	1.139	1.111	1.204
DSC (15%)	1.318	1.550	1.571	1.222	1.139	1.134	1.233
DSC (20%)	1.207	0.917	1.136	0.692	1.243	1.157	1.365
DSC (23%)	1.091	0.697	1.096	0.473	1.231	1.058	1.400
DSC (25%)	1.047	0.747	1.153	0.551	1.154	0.999	1.277
DSC (27%)	0.981	0.698	1.039	0.433	1.105	0.968	1.296
DSC (30%)	0.968	0.686	0.921	0.439	1.098	0.995	1.274
DSC (35%)	0.920	0.666	0.972	0.485	1.054	0.929	1.171

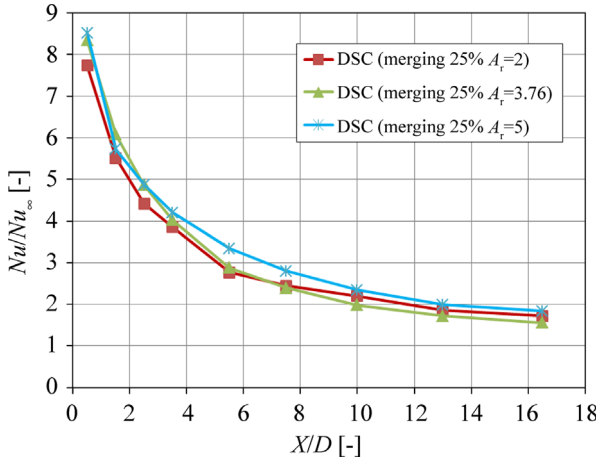

Figure 10 Comparison of circumferentially averaged Nusselt number ratio among DSC-configurations with different aspect ratios.

3.2.2. *Aspect ratio*

Figure 10 shows the circumferentially averaged Nusselt number ratio for the DSC-cooling configurations with different aspect ratios of inlet duct. It can be found in this figure that larger aspect ratio leads to larger Nusselt number ratio. A larger aspect ratio means that the fluid is closer to

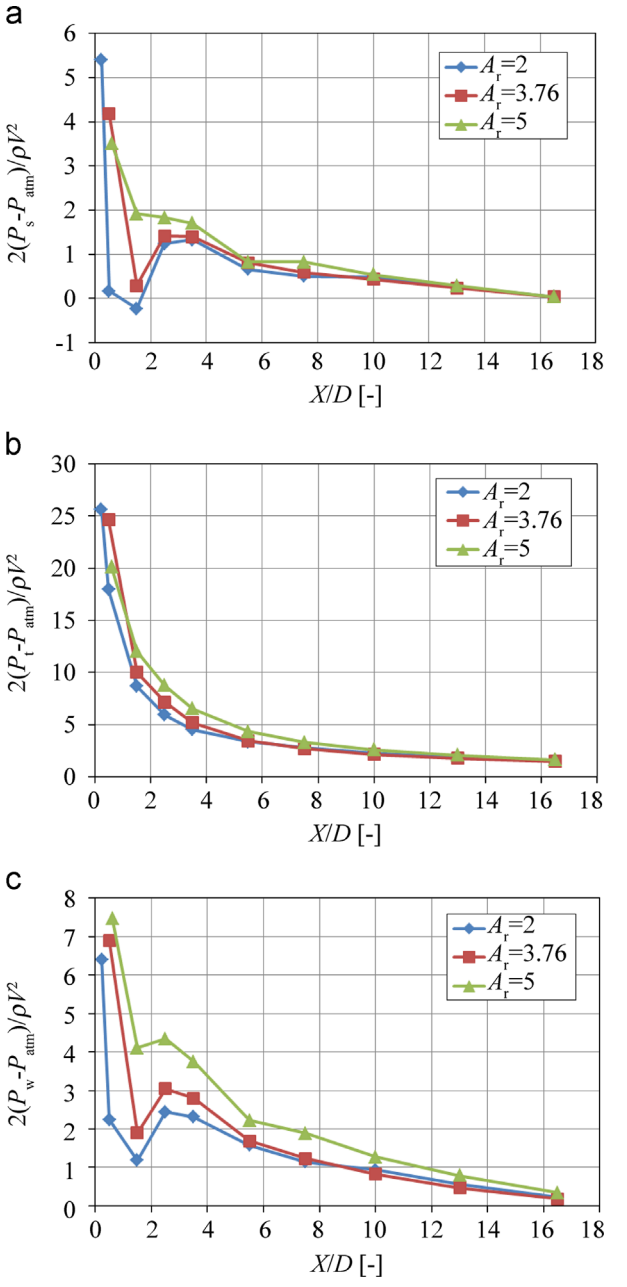

Figure 11 Pressure distributions along the axial direction. (a) Normalized static pressure, (b) normalized total pressure and (c) normalized wall static pressure for DSC-configurations with different aspect ratios.

Table 6 Comparison of Nusselt number ratio, friction factor ratio and globally-averaged thermal performance factor for DSC-configurations with different aspect ratios.

Configurations	$\overline{\overline{Nu}}/Nu_\infty$	f/f_0			$\overline{\overline{Nu}}/Nu_\infty/(f/f_0)^{1/3}$		
		Static	Total	Wall	Static	Total	Wall
SC	1	1	1	1	1	1	1
$A_r=2$	1.034	0.950	1.179	0.497	1.051	0.979	1.305
$A_r=3.76$	1.047	0.747	1.153	0.551	1.154	0.999	1.277
$A_r=5$	1.121	0.631	0.926	0.588	1.306	1.150	1.337

the chamber wall after the inlet tube; it results in higher mass density near the wall, which would in turn improve the heat transfer.

Figure 11 presents the non-dimensional static, total and wall static pressure along the axial distance from calculations with different aspect ratios. Massflow averaged static pressure and total pressure are non-dimensionalized using $\rho U^2/2$ in Figures 11(a) and (b). Circumferential surface averaged wall static pressure is non-dimensionalized using $\rho U^2/2$ in Figure 11(c). All the evaluated pressure begins from the cross section of chambers just after the inlet duct.

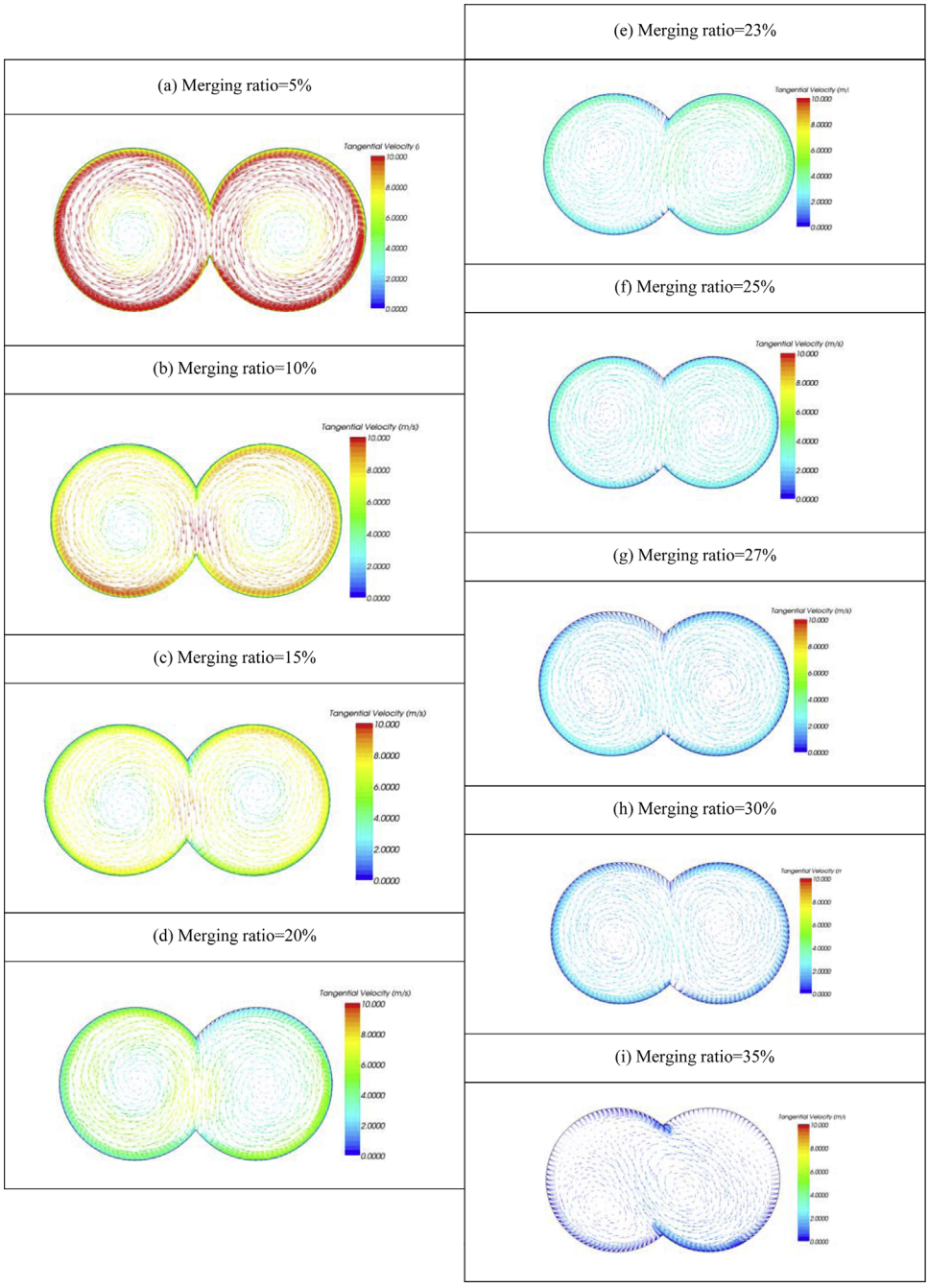

Figure A1 (a) Merging ratio=5%. (b) Merging ratio=10%. (c) Merging ratio=15%. (d) Merging ratio=20%. (e) Merging ratio=23%. (f) Merging ratio=25%. (g) Merging ratio=27%. (h) Merging ratio=30%. (i) Merging ratio=35%.

Some differences can be found at the first half length of the chamber.

Table 6 presents the calculated Nusselt number ratio, friction factor ratio and globally-averaged thermal performance of DSC-configurations with different aspect ratios in comparison with the reference SC-configuration. As shown in this table, the DSC-configuration with aspect ratio of 5 has the largest thermal performance parameter in all three pressure drop applications. It can be predicted that with further increasing of aspect ratio, the thermal performance is even better, because the mass density near the chambers wall is higher.

4. Conclusions

Aerodynamic and heat transfer enhancement of double swirl chambers cooling have been numerically investigated in the present work. The SST k-ω turbulence model, which shows the best agreement with the experimental data in validation of swirl chamber by Hay and West [5], has been chosen to calculate all the cases.

In the present study, the influence of geometry parameters, e.g. merging ratio of two chambers and aspect ratio of the inlet duct in the heat transfer augmentation and pressure drop, have been investigated. The following conclusions can be drawn:

1. In swirl flows the calculated pressure drops based on static pressure, total pressure or static wall pressure show quite different values.
2. Increasing merging ratios results in smaller Nusselt number ratio and also less pressure drop.
3. The optimal thermal performance parameter can be found with a merging ratio in the range of 20% to 23%.
4. Increased aspect ratio in inlet duct can lead to better thermal performance.

Overall, the double swirl chambers cooling shows much better thermal performance than the reference swirl chamber cooling.

Annex

Tangential velocity distribution at the section $X/D=7.5$ from calculations with different merging ratios.

See Figure A1.

References

[1] P.M. Ligrani, M.M. Oliveira, T. Blaskovich, Comparison of heat transfer augmentation techniques, AIAA Journal 41 (3) (2003) 337–362.

[2] P. Ligrani, Heat transfer augmentation technologies for internal cooling of turbine components of gas turbine engines, in: Proceedings of the 4th International Symposium Jet Propulsion and Power Engineering, Xi'an, P.R. China, September 10-12, 2012, Paper No. ISJPPE-2012-KB003.

[3] A. Ogawa, Vortex Flow, CRC Press, New York, 1993.

[4] F. Kreith, D. Margolis, Heat transfer and friction in turbulent vortex flow, Applied Scientific Research 8 (1) (1959) 457–473.

[5] N. Hay, P.D. West, Heat transfer in free swirling flow in a pipe, Journal of Heat Transfer 97 (3) (1975) 411–416.

[6] F. Chang, V.K. Dhir, Turbulent flow field in tangentially injected swirl flows in tubes, International Journal of Heat and Fluid Flow 15 (5) (1994) 346–356.

[7] F. Chang, V.K. Dhir, Mechanisms of heat transfer enhancement and slow decay of swirl in tubes using tangential injection, International Journal of Heat and Fluid Flow 16 (2) (1995) 78–87.

[8] A. Khalatov, N. Syred, P. Bowen, R. Al-Ajmi, Quasi two-dimensional cyclone-jet cooling configuration: evaluation of heat transfer and pressure losses, in: Proceedings of the 2001 International Gas Turbine and Aeroengine Congress & Exhibition, New Orleans, USA, 2001, ASME Paper GT2001-182.

[9] A. Khalatov, I. Borisov, S. Severin, V. Romanov, V. Spitsyn, Y. Dashevskyy, Heat transfer, hydrodynamics and pressure drop in the model of a blade leading edge cyclone cooling, ASME Paper GT2011-45150, 2011.

[10] A. Khalatov, N. Syred, P. Bowen, R. Al-Ajmi, A. Koylov, A. Schukin, Innovative cyclone cooling scheme for gas turbine blade: thermal-hydraulic performance evaluation, ASME Paper GT2000-237, 2000.

[11] P.M. Ligrani, C.R. Hedlund, B.T. Babinchak, R. Thambu, H.-K. Moon, B. Glezer, Flow phenomena in swirl chambers, Experiments in Fluids 24 (3) (1998) 254–264.

[12] R. Thambu, B.T. Babinchak, P.M. Ligrani, C.R. Hedlund, H.-K. Moon, B. Glezer, Flow in a simple swirl chamber with and without controlled inlet forcing, Experiments in Fluids 26 (4) (1999) 347–357.

[13] C.R. Hedlund, P.M. Ligrani, H.-K. Moon, B. Glezer, Heat transfer and flow phenomena in a swirl chamber simulating turbine blade internal cooling, Journal of Turbomachinery 121 (4) (1999) 804–813.

[14] C.R. Hedlund, P.M. Ligrani, Local swirl chamber heat transfer and flow structure at different Reynolds number, Journal of Turbomachinery 122 (2) (2000) 375–385.

[15] J.P.C.W. Ling, P.T. Ireland, N.W. Harvey, Measurement of heat transfer coefficient distributions and flow field in a model of a turbine cooling passage with tangential injection, ASME Paper GT2006-90352, 2006.

[16] Z. Liu, Z. Feng, L. Song, Numerical study of flow and heat transfer characteristics of swirl cooling on leading edge model of gas turbine blade, ASME Paper GT2011-46125, 2011.

[17] J.-J. Hwang, C.-S. Cheng, Augmented heat transfer in a triangular duct by using multiple swirling jets, Journal of Heat Transfer 121 (3) (1999) 683–690.

[18] D. Segura, S. Acharya, Internal cooling using novel swirl enhancement strategies in a slot shaped single pass channel, ASME Paper GT2010-23679, 2010.

[19] D. Segura, S. Acharya, Swirl-enhanced internal cooling of turbine blades-part 1 radial flow entry, ASME Paper GT2011-46652, 2011.

[20] D. Segura, S. Acharya, Swirl-enhanced internal cooling of turbine airfoils: part 2-90 degree flow entry, ASME Paper GT2011-46652, 2011.

[21] A. Lerch, H.-P. Schiffer, D. Klaubert, Impact on adiabatic film cooling effectiveness using internal cyclone cooling, ASME Paper GT2011-45120, 2011.

[22] F. Wassermann, S. Grundmann, M. Kloss, H.-P. Schiffer, Swirl flow investigations on the enhancement of heat transfer processes in cyclone cooling ducts, ASME Paper GT2012-69395, 2012.

[23] K. Kusterer, G. Lin, D. Bohn, T. Sugimoto, R. Tanaka, M. Kazari, Heat transfer enhancement for gas turbine internal cooling by application of double swirl cooling chambers, ASME Paper GT2013-94774, 2013.

[24] O. Kitoh, Experimental study of turbulent swirling flow in a straight pipe, Journal of Fluid Mechanics 225 (1991) 445–479.

[25] B.J. Mckeon, M.V. Zagarola, A.J. Smits, A new friction factor relationship for fully developed pipe flow, Journal of Fluid Mechanics 538 (2005) 429–443.

[26] S. Kunstmann, J. Wolfersdorf, U. Ruedel, Heat transfer and pressure loss in rectangular one-side-ribbed channels with different aspect ratios, ASME Paper GT2009-59333, 2009.

[27] G. Rau, M. Cakan, D. Moeller, T. Arts, The effect of periodic ribs on the local aerodynamic and heat transfer performance of a straight cooling channel, Journal of Turbomachinery 120 (2) (1998) 368–375.